Calcium Fluoride Nanocrystals

Molecular and Cellular MRI

International Edition: DOI: 10.1002/anie.201800838
German Edition: DOI: 10.1002/ange.201800838

Calcium Fluoride Nanocrystals: Tracers for In Vivo ^{19}F Magnetic Resonance Imaging

*Idan Ashur, Hyla Allouche-Arnon, and Amnon Bar-Shir**

Abstract: *Inorganic nanocrystals (NCs) have been extensively developed for a variety of uses. The ability to obtain high-resolution NMR signals from the core nuclei of NCs in solution could offer new opportunities in materials sciences and MR imaging. Herein, we demonstrate that small, water-soluble ^{19}F-ionic NCs can average out homonuclear dipolar interactions, enabling one to obtain high-resolution ^{19}F NMR signals in solution that reflect the MR properties of F^- in the crystal core. Decorating ^{19}F-NC surfaces with a biocompatible poly(ethylene glycol) coating maintains colloidal stability in water while preserving the NC high-resolution ^{19}F NMR properties, even after further functionalization. The high content and magnetic equivalence of the fluorides within the NCs enable their use as imaging tracers for in vivo ^{19}F MRI by facilitating a "hot-spot" display of their distribution.*

Polymers and phospholipids[1] are important components in nanoformulations designed and used in nanomedicine, but inorganic nanocrystals (NCs) have several advantages over these "soft" materials. The chemical composition, crystallinity, size, shape, surface properties, and physical characteristics of inorganic NCs[2] can be controlled, providing them with unprecedented versatility and enabling their use as nanosensors for in vivo imaging.[3] Nanoformulations designed for molecular and cellular magnetic resonance imaging (MRI) can be classified as either contrast agents or tracers.[4] Their use enables accurate coregistering of high-resolution anatomical views with subcellular information, and they are being translated into the clinic.[5] Metal-oxide-based NCs (i.e., contrast agents) exhibit supreme sensitivity[6] with controllable size,[7] shape,[8] surface modifiability,[9] metal content,[10] and variable contrast.[11,12] Nevertheless, their lack of specificity (relaxation-based MRI signal alternation) and high background signals call for background-free alternatives.

Capitalizing on the fact that ^{19}F nuclei do not exist in soft biological tissues, together with the high sensitivity of ^{19}F MRI, the ^{19}F MR signal of an introduced ^{19}F tracer can be directly monitored and presented as a quantitative "hot-spot" map over anatomical ^{1}H MRI.[13] Specifically, ^{19}F-based perfluorocarbon (PFC) nanoemulsions have been proposed as ^{19}F MRI tracers and have been successfully used in a wide range of applications,[14] including in clinical settings.[15] However, PFCs do not have the beneficial properties of inorganic NCs. For example, PFCs cannot be prepared as small (< 10 nm) formulations, and thus cannot benefit from the improved delivery and clearance capabilities of such particles.[16] Moreover, although silica coatings of PFCs have been proposed,[17] the surfaces of inorganic NCs can be readily modified through diverse and well-established synthetic procedures. The growing field of nanofluoride-based inorganic materials with unique characteristics[18] and controllable content, sizes, and shapes, creates new possibilities for ^{19}F-based formulations. However, one limiting feature of NC-based formulations is the restricted mobility of the elements within the crystal, which frequently results in NMR line broadening due to strong dipole–dipole interactions[19] and hampers their use as MRI tracers. Herein we present synthetic, water-soluble, small (< 10 nm) fluoride-based NCs that average out homonuclear dipolar interactions and thus allow high-resolution ^{19}F NMR spectroscopy of the NCs in aqueous solutions. These NCs were used for in vivo ^{19}F MRI, thus demonstrating that they combine the advantages of NCs (small, high ^{19}F equivalency, maximal ^{19}F density, surface modifiability) with the merits of ^{19}F MRI tracers.

First, we synthesized small, water-soluble, citrate-coated CaF_2 (CF-Cit) NCs (Figure 1) to examine the hypothesis that high-resolution ^{19}F NMR spectra can be obtained by sufficient averaging of homonuclear dipolar interactions of ^{19}F nuclear spins within freely tumbling fluoride-containing NCs. The obtained CF-Cit NCs were highly crystalline (Figure 1 a)

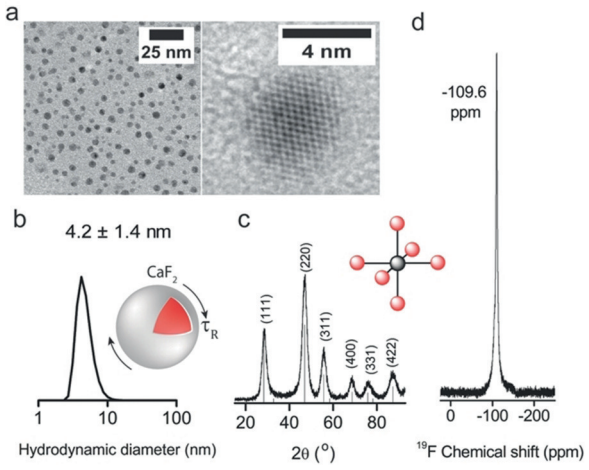

Figure 1. Water-soluble citrate-coated CaF_2 NCs. a) TEM images. b) DLS histogram. c) XRD pattern with a schematic illustration of the first coordination sphere of Ca^{2+}. d) High-resolution ^{19}F NMR spectrum in aqueous solution.

[*] Dr. I. Ashur, Dr. H. Allouche-Arnon, Dr. A. Bar-Shir
Department of Organic Chemistry
The Weizmann Institute of Science
7610001 Rehovot (Israel)
E-mail: amnon.barshir@weizmann.ac.il
Supporting information and the ORCID identification number(s) for the author(s) of this article can be found under: https://doi.org/10.1002/anie.201800838.

and monodisperse (see Figure S1 in the Supporting Information). Energy-dispersive X-ray spectroscopy (EDS) analysis revealed an approximately 1:2 ratio of Ca^{2+} to F^- ions (see Figure S2), and the NCs preserved monodispersity in water, as determined by dynamic light scattering (DLS, Figure 1b). The XRD pattern of the synthetic CF-Cit NCs (Figure 1c) features a typical cubic-phase, fluorite-type structure, which was supported by FFT analysis of the TEM image of a single particle (see Figure S3). Then, the water-soluble CF-Cit NCs were studied by high-resolution ^{19}F NMR spectroscopy in water (Figure 1d). In a face-centered cubic (fcc) structure of CaF_2, all fluorides were expected to be magnetically equivalent, as reflected by the first coordination sphere scheme (inset, Figure 1c). Indeed, a singlet peak was observed in the high-resolution ^{19}F NMR spectrum at −109.6 ppm, similar to the frequency observed for CaF_2 powder by solid-state NMR spectroscopy.[20] This singlet peak is an advantage when proposing novel ^{19}F-based tracers for ^{19}F MRI applications, for which high magnetic equivalence of the ^{19}F source is desired for maximizing ^{19}F MR signal intensity.[14a,21]

To confirm that the fcc structure of fluoride NCs is crucial for obtaining a highly intense singlet peak in high-resolution ^{19}F NMR experiments, two additional water-soluble nanofluorides were synthesized (Figure 2). Citrate-coated water-soluble SrF_2 NCs (Figure 2a), with a similar fcc crystal structure to that of CaF_2 (Figure 2b), also feature a clear, single high-resolution ^{19}F NMR peak in water (Figure 2c). Conversely, an aqueous solution of small monodispersed citrate-coated LaF_3 NCs (Figure 2d), with a tysonite-type crystal structure (Figure 2e), exhibited a more complex high-resolution ^{19}F NMR spectrum in water. This spectrum (Figure 2f) depicts more than one ^{19}F resonance with the expected chemical shifts obtained in solid-state ^{19}F NMR studies of LaF_3 crystals, reflecting fluorides at nonequivalent crystallographic sites.[20,22]

To facilitate the use of nanofluorides in vivo, we developed and synthesized poly(ethylene glycol) (PEG)-coated CaF_2 NCs (Figure 3) with the aim of providing solubility,

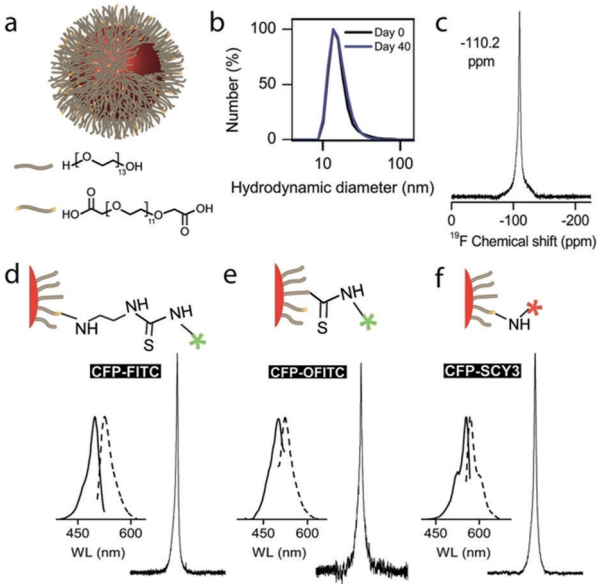

Figure 3. Water-soluble PEGylated CaF_2 NCs. a) Illustration of the PEGylated CaF_2 NCs (CFP). b) DLS histograms. c) High-resolution ^{19}F NMR spectrum in aqueous solution. d–f) Fluorescence spectra and high-resolution ^{19}F NMR spectra of functionalized CFP NCs. Green and red stars represent FITC and SCY3 functional groups conjugated to the CFP NC, respectively.

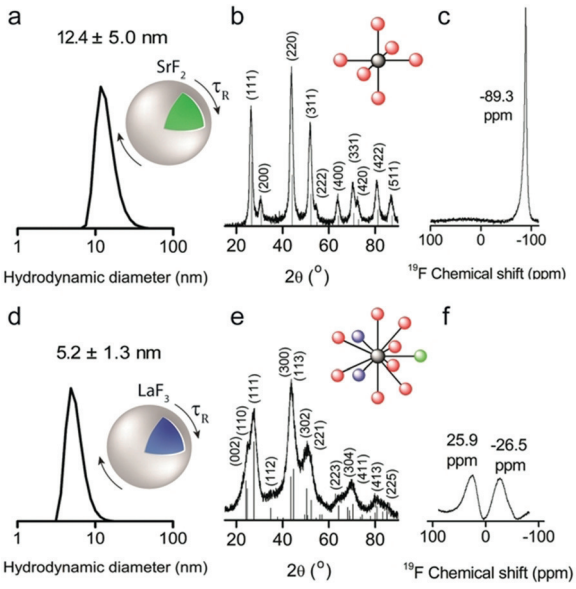

Figure 2. Water-soluble SrF_2 and LaF_3 NCs. a,d) DLS histograms of Cit-SrF_2 (a) and Cit-LaF_3 (d). b,e) XRD patterns of Cit-SrF_2 (b) and Cit-LaF_3 (e); schematic illustrations of the first coordination sphere of Sr^{2+} and the La^{3+} are shown as insets in (b) and (e), respectively. c,f) High-resolution ^{19}F NMR spectra of Cit-SrF_2 and Cit-LaF_3 NCs, respectively, in aqueous solution.

stability, monodispersity, and surface modifiability.[23] The CaF_2–PEG (CFP) NCs were synthesized by a solvothermal approach with a mixture of PEG-hydroxyl and PEG-carboxylate (average MW 600), purified, and characterized by TEM, XRD, EDS, ^1H and ^{13}C NMR spectroscopy, FTIR spectroscopy, and thermogravimetric analysis (TGA; see Figures S4–S10). The DLS histograms of CFP NCs in aqueous solution indicate that the small particles are monodisperse with colloidal stability retained for at least 40 days (Figure 3b). High-resolution ^{19}F NMR experiments of CFP NCs in aqueous solution revealed a clear singlet peak at the expected chemical shift of CaF_2 (Figure 3c). To demonstrate the feasibility of chemically modifying the CFP for future applications, we further functionalized the CFP NCs with fluorescent moieties (for a description of the synthesis, see the Supporting Information). Both fluorescein isothiocyanate (FITC) and sulfo-cyanine3 (SCY3) were used to demonstrate the feasibility of CFP functionalization (Figure 3d–f). In all cases, the high-resolution ^{19}F NMR properties of the modified NCs were preserved along with high fluorescence (Figure 3f–h), used to monitor uptake of NCs by live cells (see Figure S11). The DLS histograms of all functionalized CFP NCs in aqueous solution showed colloid monodispersity that was stable for several weeks (see Figure S12 and Table S1 in the Supporting Information).

The longitudinal (T_1) and transverse (T_2) relaxation times of the ^{19}F within the CFP NCs were determined to optimize the acquisition parameters for future ^{19}F MRI experiments (Figure 4a; for similar measurements with CF-Cit, see Figure S14 and Table S2). The relatively long T_1 time of CFP may be less favorable for MRI applications owing to the long repetition time (TR) needed to fulfil the $5 \times T_1$ condition for maximizing the MR signal. However, by using low-flip-angle excitation pulses it was possible to significantly shorten the TR used, allowing increased averaging and thus a higher signal-to-noise-ratio (SNR) for a given experiment time. The ^{19}F MR signal of CFP could be maximized at low flip angles (Ernst angle) at a fixed experiment time, while a very low SNR was obtained when a 90° pulse was used ($TR = 5 \times T_1 = 48.5$ s; Figure 4b). The addition of a paramagnetic dopant into the NCs should be considered for the purpose of shortening T_1, as proposed for PFC nanoemulsions.[25] Although until recently nuclear spins with relatively short T_2 values could not be monitored with conventional MRI acquisition schemes, ultrashort echo time (UTE) and zero echo time (ZTE) pulse sequences enable MRI of nuclear spin pools with an extremely short T_2 value,[24] including metallated PFCs with ^{19}F MRI.[25]

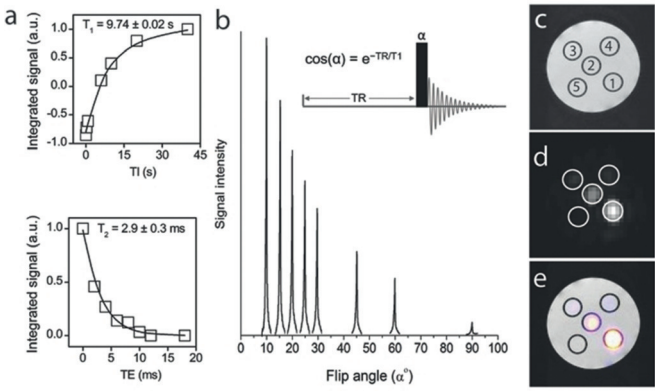

Figure 4. CFP relaxation properties and ^{19}F MRI. a) ^{19}F NMR signal of CFP NCs as a function of inversion time (TI, upper panel) or echo time (TE, bottom panel), used to calculate T_1 and T_2 values, respectively. b) ^{19}F NMR signal as a function of the flip angle (α) obtained from 3 min experiment time. c–e) MRI phantom containing CFP NCs with different concentrations (total F^-): 1) 250, 2) 75, 3) 25, 4) 5, and 5) 2.5 mM; c) ^1H MRI; d) ^{19}F MRI (TE = 25 μs); e) display of ^{19}F data as a "hot-spot" map on a ^1H MR image.

Next, the feasibility of spatially mapping the distribution of our newly developed water-soluble nanofluorides with ^{19}F MRI was examined. A phantom composed of samples containing CFP at a range of concentrations was prepared and imaged with a 9.4 T MRI scanner (Figure 4c–e). As expected, no difference was observed between the four tubes using ^1H MRI (Figure 4c). However, by using the UTE sequence, which enables MRI of nuclear spin pools with an extremely short T_2 value, a clear ^{19}F MR signal could be observed from the CFP-containing tubes (Figure 4d). These data were acquired with an echo time (TE) of 25 μs (TR = 50 ms with a flip angle of 5.7° to achieve Ernst angle conditions) and allow a "hot-spot" representation of the distributions of nanofluorides, thus demonstrating their potential to be used as imaging tracers for MRI applications (Figure 4e). Importantly, ^{19}F MR images acquired with a gradient-echo-based sequence (TE = 3.1 ms; see Figure S16) did not reveal any ^{19}F signal from the CFP samples, thus reflecting the necessity of using extremely short echo times when acquiring ^{19}F MR images of nanofluorides. This ability to monitor extremely short T_2 values with conventional MRI setups (UTE-based acquisition schemes) offers new opportunities for the design and development of novel inorganic NCs as X-nuclei MRI tracers.

It is frequently useful to obtain information from multiple imaging agents (or targets) simultaneously and present this information as a multicolor map. MRI signals of different nanofluorides (i.e. CaF_2 and SrF_2) can be color-encoded based on the difference between their ^{19}F NMR chemical shifts (Figures 1 and 2) and displayed in a multiplexed manner (Figure 5; see also Figure S17). The ^{19}F NMR chemical shift of CaF_2 (ca. −109 ppm) differs from that of PFC-based nanoemulsions as well and therefore allows the combination of CaF_2 and PFC in future multicolor studies differentiating between these two nanoformulations while in the same field of view (see Figure S18). The favorable relaxation properties of PFCs for ^{19}F MRI result in a higher SNR as compared to nanofluorides, when comparing the same ^{19}F content within the studied samples (see Figure S18). However, by using nanofluorides a much higher ^{19}F payload per nanoparticle can be achieved (27–71 % more ^{19}F per particle for CaF_2 NCs as compared to PFC; see Table S4 and related equations and text). In principle, by using ^{19}F-NCs other than CaF_2 (e.g., MgF_2) an even larger ^{19}F/particle payload could be achieved (see Table S4).

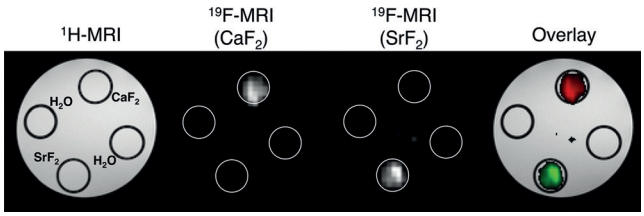

Figure 5. Artificial "multicolor" ^{19}F MR imaging. A phantom composed of two tubes containing water and two tubes containing either CaF_2 or SrF_2 NCs were used. From left to right: ^1H MRI, ^{19}F-UTE MRI (O_1 set to the frequency offset of CaF_2), ^{19}F-UTE MRI (O_1 set to the frequency offset of SrF_2), multicolor map overlaid on the ^1H MR image with CaF_2 (red) and SrF_2 (green) ^{19}F MR signals.

Finally, the potential of using the proposed ^{19}F-NCs (specifically, CFP-SCY3, Figure 3f) as imaging tracers for in vivo ^{19}F MRI was evaluated in a mouse model of inflammation. Cellular toxicity of the CFP-SCY3 NCs as well as their ability to be taken up by macrophages was evaluated prior to in vivo MRI experiments (see Figures S15 and S11, respectively). Ten days post-immunization, when extensive inflammatory activity is expected, mice were subjected to MRI sessions that acquired pre- and post-injection of CFP-SCY3 NCs.

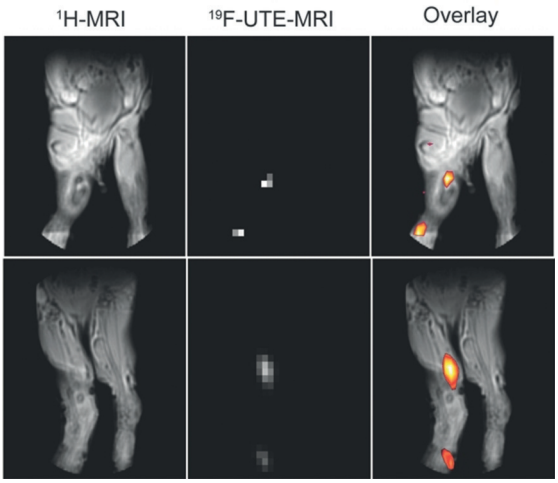

Figure 6. In vivo imaging of PEGylated CaF_2. Anatomical ^{1}H MRI of two representative mice (left-hand images) and matched ^{19}F MRI (middle images) shown as pseudocolor maps overlaid on the anatomical ^{1}H MR images (right-hand images). Mice were subjected to injection of CFP-SCY3 (80 µL into mouse footpads), and the ^{19}F MRI scan time was 1 h (TR/TE = 150/0.02 ms).

A clear ^{19}F signal was observed at the region of the popliteal lymph node (LN) of mice injected with NCs ($N = 4$) within the same leg as the injection site (Figure 6) 1 h post-injection. Tracers of the ^{19}F MR signal could be observed at the injection site (Figure 6, middle and right panels, bottom ^{19}F MR signal) with no ^{19}F MR signal observed from contralateral regions. These results, showing that injected nanofluorides accumulate in the LN of inflamed mice, are in good agreement with previous observations of small inorganic NCs draining into the LN of the injected leg of inflamed subjects following subcutaneous injection.[26]

In summary, we have demonstrated that small fluoride-based NCs freely tumbling in solution can be studied by high-resolution ^{19}F NMR spectroscopy and be used as nanotracers for direct and real-time in vivo ^{19}F MRI. The growing interest in fluoride-based nanomaterials for biological sciences and nanomedicine,[27] coupled with the strengths of ^{19}F-MRI, called for novel fluorine imaging agents. The ^{19}F-NC platform described herein fills this gap by introducing a new type of ^{19}F tracer with advantageous size, maximal ^{19}F density, and surface modifiability. The enhanced performance of these nanofluorides suggests utility in a wide range of applications.

Acknowledgements

This project received funding from the European Research Council (ERC) under the Horizon 2020 research and innovation program of the European Union (grant agreement No. 677715).

Conflict of interest

The authors declare no conflict of interest.

Keywords: cellular imaging · fluorine · magnetic resonance imaging · nanofluorides · nanoparticles

How to cite: *Angew. Chem. Int. Ed.* **2018**, *57*, 7478–7482
Angew. Chem. **2018**, *130*, 7600–7604

[1] a) J. W. Hickey, J. L. Santos, J. M. Williford, H. Q. Mao, *J. Controlled Release* **2015**, *219*, 536–547; b) T. M. Allen, P. R. Cullis, *Adv. Drug Delivery Rev.* **2013**, *65*, 36–48.
[2] Y. Yin, A. P. Alivisatos, *Nature* **2005**, *437*, 664–670.
[3] a) X. Michalet, F. F. Pinaud, L. A. Bentolila, J. M. Tsay, S. Doose, J. J. Li, G. Sundaresan, A. M. Wu, S. S. Gambhir, S. Weiss, *Science* **2005**, *307*, 538–544; b) J. W. Bulte, T. Douglas, B. Witwer, S. C. Zhang, E. Strable, B. K. Lewis, H. Zywicke, B. Miller, P. van Gelderen, B. M. Moskowitz, I. D. Duncan, J. A. Frank, *Nat. Biotechnol.* **2001**, *19*, 1141–1147; c) O. Rabin, J. Manuel Perez, J. Grimm, G. Wojtkiewicz, R. Weissleder, *Nat. Mater.* **2006**, *5*, 118–122; d) M. F. Kircher, A. de la Zerda, J. V. Jokerst, C. L. Zavaleta, P. J. Kempen, E. Mittra, K. Pitter, R. Huang, C. Campos, F. Habte, R. Sinclair, C. W. Brennan, I. K. Mellinghoff, E. C. Holland, S. S. Gambhir, *Nat. Med.* **2012**, *18*, 829–834; e) D. P. Cormode, E. Roessl, A. Thran, T. Skajaa, R. E. Gordon, J. P. Schlomka, V. Fuster, E. A. Fisher, W. J. Mulder, R. Proksa, Z. A. Fayad, *Radiology* **2010**, *256*, 774–782; f) B. Gleich, J. Weizenecker, *Nature* **2005**, *435*, 1214–1217.
[4] E. T. Ahrens, J. W. Bulte, *Nat. Rev. Immunol.* **2013**, *13*, 755–763.
[5] J. W. Bulte, *Am. J. Roentgenol.* **2009**, *193*, 314–325.
[6] E. M. Shapiro, S. Skrtic, K. Sharer, J. M. Hill, C. E. Dunbar, A. P. Koretsky, *Proc. Natl. Acad. Sci. USA* **2004**, *101*, 10901–10906.
[7] J. Park, E. Lee, N. M. Hwang, M. Kang, S. C. Kim, Y. Hwang, J. G. Park, H. J. Noh, J. Y. Kim, J. H. Park, T. Hyeon, *Angew. Chem. Int. Ed.* **2005**, *44*, 2872–2877; *Angew. Chem.* **2005**, *117*, 2932–2937.
[8] Z. Zhao, Z. Zhou, J. Bao, Z. Wang, J. Hu, X. Chi, K. Ni, R. Wang, X. Chen, Z. Chen, J. Gao, *Nat. Commun.* **2013**, *4*, 2266.
[9] R. Weissleder, K. Kelly, E. Y. Sun, T. Shtatland, L. Josephson, *Nat. Biotechnol.* **2005**, *23*, 1418–1423.
[10] J. H. Lee, Y. M. Huh, Y. W. Jun, J. W. Seo, J. T. Jang, H. T. Song, S. Kim, E. J. Cho, H. G. Yoon, J. S. Suh, J. Cheon, *Nat. Med.* **2007**, *13*, 95–99.
[11] T. Kim, E. Momin, J. Choi, K. Yuan, H. Zaidi, J. Kim, M. Park, N. Lee, M. T. McMahon, A. Quinones-Hinojosa, J. W. Bulte, T. Hyeon, A. A. Gilad, *J. Am. Chem. Soc.* **2011**, *133*, 2955–2961.
[12] S. Laurent, D. Forge, M. Port, A. Roch, C. Robic, L. Vander Elst, R. N. Muller, *Chem. Rev.* **2008**, *108*, 2064–2110.
[13] a) U. Flögel, E. T. Ahrens, *Fluorine Magnetic Resonance Imaging*, Pan Stanford Publishing Pte. Ltd, Singapore, **2016**; b) E. T. Ahrens, J. Zhong, *NMR Biomed.* **2013**, *26*, 860–871; c) J. Ruiz-Cabello, B. P. Barnett, P. A. Bottomley, J. W. Bulte, *NMR Biomed.* **2011**, *24*, 114–129; d) I. Tirotta, V. Dichiarante, C. Pigliacelli, G. Cavallo, G. Terraneo, F. B. Bombelli, P. Metrangolo, G. Resnati, *Chem. Rev.* **2015**, *115*, 1106–1129.
[14] a) E. T. Ahrens, R. Flores, H. Xu, P. A. Morel, *Nat. Biotechnol.* **2005**, *23*, 983–987; b) U. Flogel, Z. Ding, H. Hardung, S. Jander, G. Reichmann, C. Jacoby, R. Schubert, J. Schrader, *Circulation* **2008**, *118*, 140–148; c) J. M. Janjic, M. Srinivas, D. K. Kadayakkara, E. T. Ahrens, *J. Am. Chem. Soc.* **2008**, *130*, 2832–2841; d) J. Ruiz-Cabello, P. Walczak, D. A. Kedziorek, V. P. Chacko, A. H. Schmieder, S. A. Wickline, G. M. Lanza, J. W. Bulte, *Magn. Reson. Med.* **2008**, *60*, 1506–1511.
[15] E. T. Ahrens, B. M. Helfer, C. F. O'Hanlon, C. Schirda, *Magn. Reson. Med.* **2014**, *72*, 1696–1701.
[16] M. Yu, J. Zheng, *ACS Nano* **2015**, *9*, 6655–6674.
[17] a) H. Matsushita, S. Mizukami, F. Sugihara, Y. Nakanishi, Y. Yoshioka, K. Kikuchi, *Angew. Chem. Int. Ed.* **2014**, *53*, 1008–1011; *Angew. Chem.* **2014**, *126*, 1026–1029; b) T. Nakamura, F.

Sugihara, H. Matsushita, Y. Yoshioka, S. Mizukami, K. Kikuchi, *Chem. Sci.* **2015**, *6*, 1986 – 1990.
[18] a) G. Chen, J. Shen, T. Y. Ohulchanskyy, N. J. Patel, A. Kutikov, Z. Li, J. Song, R. K. Pandey, H. Agren, P. N. Prasad, G. Han, *ACS Nano* **2012**, *6*, 8280 – 8287; b) H. X. Mai, Y. W. Zhang, R. Si, Z. G. Yan, L. D. Sun, L. P. You, C. H. Yan, *J. Am. Chem. Soc.* **2006**, *128*, 6426 – 6436; c) S. Sivakumar, F. C. van Veggel, M. Raudsepp, *J. Am. Chem. Soc.* **2005**, *127*, 12464 – 12465; d) F. Wang, Y. Han, C. S. Lim, Y. Lu, J. Wang, J. Xu, H. Chen, C. Zhang, M. Hong, X. Liu, *Nature* **2010**, *463*, 1061 – 1065.
[19] L. E. Marbella, J. E. Millstone, *Chem. Mater.* **2015**, *27*, 2721 – 2739.
[20] A. Sadoc, M. Body, C. Legein, M. Biswal, F. Fayon, X. Rocquefelte, F. Boucher, *Phys. Chem. Chem. Phys.* **2011**, *13*, 18539 – 18550.
[21] I. Tirotta, A. Mastropietro, C. Cordiglieri, L. Gazzera, F. Baggi, G. Baselli, M. G. Bruzzone, I. Zucca, G. Cavallo, G. Terraneo, F. Baldelli Bombelli, P. Metrangolo, G. Resnati, *J. Am. Chem. Soc.* **2014**, *136*, 8524 – 8527.
[22] A. Y. Lo, V. Sudarsan, S. Sivakumar, F. van Veggel, R. W. Schurko, *J. Am. Chem. Soc.* **2007**, *129*, 4687 – 4700.
[23] A. S. Karakoti, S. Das, S. Thevuthasan, S. Seal, *Angew. Chem. Int. Ed.* **2011**, *50*, 1980 – 1994; *Angew. Chem.* **2011**, *123*, 2024 – 2040.
[24] M. D. Robson, P. D. Gatehouse, M. Bydder, G. M. Bydder, *J. Comput. Assist. Tomogr.* **2003**, *27*, 825 – 846.
[25] A. A. Kislukhin, H. Xu, S. R. Adams, K. H. Narsinh, R. Y. Tsien, E. T. Ahrens, *Nat. Mater.* **2016**, *15*, 662 – 668.
[26] G. Niu, X. Chen, *Theranostics* **2015**, *5*, 686 – 697.
[27] G. Chen, H. Qiu, P. N. Prasad, X. Chen, *Chem. Rev.* **2014**, *114*, 5161 – 5214.

Manuscript received: January 21, 2018
Accepted manuscript online: March 8, 2018
Version of record online: March 30, 2018

